pss-Header will be provided by the publisher

Green electroluminescence of Al/Tb/Al/SiO_2 devices fabricated by electron beam evaporation

J. L. Frieiro[1], O. Blázquez[1], J. López-Vidrier[1,2], L. López-Conesa[1], S. Estradé[1], F. Peiró[1], J. Ibáñez[1], S. Hernández[1], and B. Garrido[1]

[1] MIND–IN[2]UB, Department of Engineering: Electronics, Universitat de Barcelona, Martí i Franquès 1, E-08028 Barcelona, Spain
[2] IMTEK, Faculty of Engineering, Albert-Ludwigs-University, Freiburg, Georges-Köhler-Allee 103, D-79110 Freiburg (Germany).
[3] Institute of Earth Sciences Jaume Almera, ICTJA-CSIC, Lluís Soler i Sabarís s/n, E-08028 Barcelona, Catalonia, (Spain)

Received ZZZ, revised ZZZ, accepted ZZZ
Published online ZZZ (Dates will be provided by the publisher.)
Keywords Please provide about four verbal keywords for your manuscript.

In this work, the fabrication and the structural, optical and electrical properties of Al-Tb/SiO_2 nanomultilayers have been studied. The nanomultilayers were deposited by means of electron beam evaporation on top of p-type Si substrates. Optical characterization shows a narrow and strong emission in the green spectral range, indicating the optical activation of Tb^{3+} ions. The electrical characterization revealed conduction limited by the electrode, although trapped-assisted mechanisms can also contribute to transport. The electroluminescence analysis revealed also emission from Tb^{3+} ions, yielded promising results to include this material in future optoelectronics applications as integrated emitting devices.

1 Introduction The invention of LEDs has opened the door for the field of optoelectronics, as the use of semiconductors allows scaling these light sources to the sizes of microelectronic devices employed today. Optoelectronic devices are designed to employ light in combination with (or instead of) electric currents, which introduces many advantages: separation of electronic devices (thus enabling the optimization of the chip layout), reduction of electromagnetic interference, cable length and weight, sustenance of precise signal timing, reduction of interconnect densities and energy saving (thanks to lower heat losses) [1]–[4].

These new devices need to be able to operate in concert with current electronic devices based on silicon technology, which requires of Si-based light collectors, transducers between electric and optical signals, light waveguides, and light emitters. For the latter, semiconductor materials doped with rare earth (RE) ions have been widely studied in the last two decades due to their narrow and intense luminescence, as a potential alternative for more efficient devices than LEDs [5]–[7].

Rare earth elements have their 4*f* electronic shell partially filled and when they are optically active, they usually have an oxidation state +3 due to the loss of one 4*f* electron and the two 6*s* electrons. These elements have luminescent properties resulting from the intra-4*f* transitions (almost independent of the matrix) or 5*d*-to-4*f* (sensitive to the matrix). [8]

Erbium has been studied as dopant of different films like silica (SiO_2), yielding emissions in the infrared part of the spectrum (~1535 nm) when in an Er^{3+} oxidation state, which makes it very useful for optical fiber telecommunication systems [9], [10]. Other REs have been researched for their emission in the visible range, such as Ce^{3+} [8], Tb^{3+} [11] and Eu^{3+} [12]; in the blue (460nm), green (543 nm) and red (615 nm) parts of the spectra respectively. In the Fig. 1, the electronic levels, energies and transitions for a particular RE species (Tb^{3+} ions as it will be later study in this work [13]) are presented.

Fabrication of these materials has been exploited through many different techniques, such as plasma-enhanced chemical vapor deposition [11], ion implantation [14], liquid source chemical vapor deposition [15], magnetron sputtering [16] and sol-gel [17]. Some other techniques have also been attempted, but are less commonly employed, like atomic layer deposition [18].

Following the approach to new RE light emitters, in this work it is described the fabrication and characterization of nanomultilayered (NML) structures composed of SiO_2, Al and Tb^{3+} ions, by means of electron beam evaporation (EBE). In a previous work, different combinations of these layers have been tested aiming at the best layer configuration that exhibits stronger emission [19]. The optical properties of the chosen configuration were studied by photoluminescence (PL) in samples annealed at different temperatures [20].

The films employed in this work were deposited by using EBE, considering the optimum nanomultilayered structure as Al-Tb/SiO_2, on top of a *p*-type Si substrate. The films used for the structural and optical characterization consist of 15×Al/Tb/Al/SiO_2 layers, ending on a SiO_2 layer that serves as protection. For the electrical characterization, 5×Al/Tb/Al/SiO_2 layers were fabricated, also on a *p*-type Si substrate, adding a full area bottom electrode of Al and top contact of indium tin oxide (ITO). The ITO contact also allows for electro-optical characterization, as it is a transparent conducting oxide (TCO). The average compo-

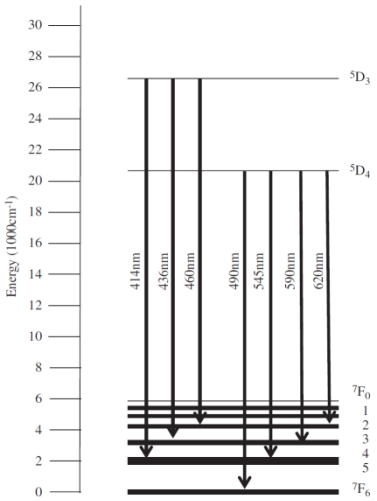

Figure 1 Electronic transitions of Tb^{3+}, taken from Ref. [13].

sition of the nanomultilayers was assessed by using X-ray photoelectron spectroscopy (XPS). Different techniques were employed to determine the optical properties of the Tb-films, using PL and cathodoluminescence (CL). The electrical properties were studied through the different *I*(*V*) curves obtained. Finally, the electroluminescence (EL) of the NMLs was also measured in the accumulation regime. The results suggest the possibility of employing EBE for fabrication of RE-doped materials that can be introduced into devices for optoelectronic applications in the future.

2 Experimental details

Different combinations in nanomultilayer structures for SiO_2, Al and Tb were tested in a previous study, in order to achieve the optimal configuration for the optical activation of the Tb^{3+} ions [19], [20]. All test samples and the ones here employed were fabricated by electron beam evaporation, and deposited on top of *p*-type Si substrates, which were cleaned with acetone, isopropyl alcohol, ethanol, and de-ionized water, and agitated ultrasonically during each process, before been introduced into the chamber.

The equipment employed for the deposition is a PFEIFFER VACUUM Classic 500 chamber with a Ferrotec GENIUS electron beam controller and a Ferrotec CARRERA high-voltage power supply. The base pressure in the chamber was 1.6×10^{-6} mbar and the temperature of the substrate was kept at 100 °C. Acceleration voltages were 6 kV for SiO_2 and Tb, and 10 kV for Al, with deposition rates of 1.0 Å/s, 0.2 Å/s and 0.2 Å/s, respectively.

The samples for the structural and optical characterization consisted of 15 stacks of Al/Tb/Al/SiO_2, with two 10-nm layers of SiO_2 before and after them to prevent any atomic diffusion from or to the nanomultilayers. The nominal thickness of the Al, Tb and SiO_2 layer were 0.8, 0.4 and 3 nm, respectively [see Fig. 2(a) and Fig. 2(b)]. After deposition, the samples were submitted to an annealing process at 1100 °C in N_2 atmosphere for 1 hour. An identical sample was also fabricated but with no Al, in order to observe the influence of this atomic specie. In the Fig. 2(a) the cross-section of the nanomultilayers acquired by transmission electron microscopy (TEM) is shown, where the nanometric structure can be clearly seen: the bright layers with a thickness of 5 nm correspond to SiO_2, whereas the dark ones, with a thickness of 3 nm, are a stack of Al-Tb, as demonstrated by electron energy loss spectroscopy [20]. As revealed by the TEM image, this stack serves as delta doping system of Tb in an Al/SiO_2 matrix, allowing to obtain nanometric separation between the Tb ions and avoiding their clustering.

For the electrical and electro-optical characterization, new samples were fabricated consisting in 5 stacks of Al/Tb/Al/SiO_2, also annealed at 1100 °C in N_2 atmosphere for 1 hour. After annealing, indium tin oxide (ITO) electrodes were deposited on top of the multilayers using a shadow mask, with circular shape with a radius of 200 µm, and subsequently annealed at 600 °C in N_2 atmosphere for 1 hour. Finally, a full area Al metallization was performed on the backside of the Si substrate for defining the bottom contact. This structure is schematically shown on Fig. 2 (c).

To determine the overall composition of the deposited films, XPS measurements were carried out using a PHI 5500 Multitechnique System, thus obtaining information regarding the Al influence on the Tb-related binding formation.

Photoluminescence measurements with two different excitation energies were employed for determining the optically active emission from Tb^{+3} ions. The 325-nm line from a HeCd laser or the 488.0-nm line from an Ar^+ laser were used for the excitation of the Tb^{3+} ions. In the case of the HeCd laser, the spectra were analyzed using a Horiba

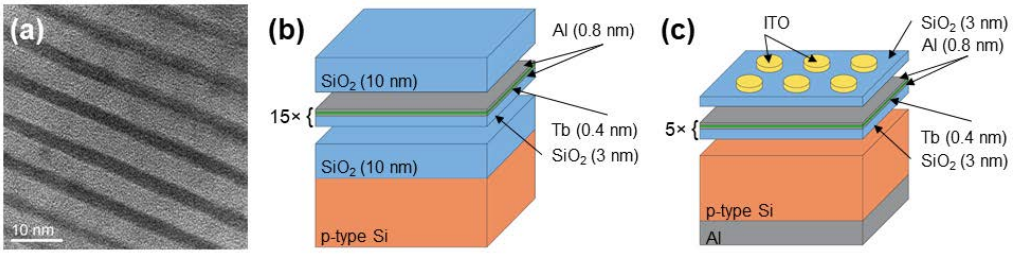

Figure 2 (a) HRTEM image of the deposited nanomultilayer structure, and sketch of the deposited structures: (b) for structural and optical characterization and (c) for electrical and electro-optical characterization.

Jobin Yvon LabRAM HR spectrometer, whereas the spectral analysis exciting with the Ar^+ laser was done using a GaAs photomultiplier tube (PMT) coupled to a monochromator in a lock-in configuration. For the acquisition of CL spectra, a JEOL JSM-7100F scanning electron microscope coupled to a monochromator and a GaAs PMT were employed. In order to avoid damage on the surface, a defocused electron beam of 80 μA, accelerated at 2 keV, was used for the measurements.

Electrical characterization of the samples was done by 2 contact measurements with an Agilent B1500 semiconductor device analyzer and a Cascade Microtech Summit 11000 probe station using a Faraday cage. The back-contact was grounded through the chuck, whereas the top ITO-contact was swept from -15 V to 15 V, with steps of 50 mVs^{-1}.

Emission from the sample obtained through electroluminescence (EL) was collected with a Seiwa 888 L microscope. Whereas the integrated emission was recorded using the same GaAs PMT employed in the PL measurements, the spectral emission was captured by means of Princeton Instruments LN-cooled charge-coupled device via a 1/4m Oriel monochromator.

3 Results and discussion

Measurements performed by XPS allowed determining the composition and the effect of the presence of Al atoms surrounding the Tb ions. In table I we have summarized the obtained results. Whereas the sample with no Al showed stoichiometric SiO_2, the sample containing Al showed an increase of the oxygen content. Thus, the Tb ions in the sample with no Al may be bound to other Tb ions or dangling bounds from SiO_2. On the other hand, the oxygen excess in the sample with Al is probably bound to Al forming alumina (Al_2O_3) with all the Al atoms oxidized, and the remaining oxygen forms Tb_2O_3 (Tb ions are less reactive than Al ones). In this case, we found a 45% of the Tb atoms to be forming this oxide. Thus, the addition of Al contributes to the oxidation of Tb ions, which will influence also their emission properties [20].

Table 1 XPS evaluated atomic compositions for the Tb/SiO_2 and $Al/Tb/Al/SiO_2$ NMLs.

	Atomic content (%)			
	Si	O	Tb	Al
Tb/SiO_2	33	65	2	-
$Al/Tb/Al/SiO_2$	24	65	1	10

Optical emission of the $Al/Tb/Al/SiO_2$ structure was first characterized by means of PL. Two different excitation lines were employed: one of λ = 325 nm and another of λ = 488 nm (see Fig. 3). The spectrum acquired with the 325-nm line shows peaks at 489, 542, 584 and 621 nm. When using the 488 nm line, the same emissions were detected but the one at 489 nm, as it is close to the excitation wavelength. These emission bands are a consequence of the intra-4*f* electronic radiative transitions ($^5D_4 \rightarrow {}^7F_J$, with J = 6, 5, 4 and 3) [8].

Similar emission as for PL was obtained when performing CL measurements, exciting the sample with an electron beam of 2 keV. Figure 3 shows the emission spectrum collected with the characteristic peaks of Tb^{3+} at 489, 544, 587 and 624 nm. These emission bands correspond with the transitions $^5D_4 \rightarrow {}^7F_J$ as previously described. Blue emission bands also appear in the CL spectrum, corresponding to $^5D_3 \rightarrow {}^7F_J$ (J = 5 and 4) transitions, with peaks at 415 and 437 nm. All these results are in good agreement with others found in the literature (see Ref. 21).

The most intense emission at 544 nm in both PL and CL spectra corresponds to the green visible range, and it is split into two peaks, as a consequence of the Stark effect due to the local electric field [8]. These results evidence that the employed deposition technique and methodology, that takes advantage of the nanomultilayered deposition of different materials, produce optically active Tb^{3+} species, emitting in the green spectral region.

The electrical properties of the fabricated devices were analyzed by acquiring the $I(V)$ curves, grounding the Al bottom electrode with the chuck whereas the ITO contact on top was swept in two regimes: accumulation (negative bias) and inversion (positive bias). The obtained curves for each regime are displayed in Fig. 4. The devices can reach intensities in the order of 10^2 μA at -15 V applied voltage. Higher voltages were not sustained by the ITO contacts as the current increased to mA. The curves show an almost symmetric behavior for both regimes, indicating non-rectifying characteristics.

As shown by structural characterization, the device is composed by layers of SiO_2 and Al_2O_3, for which an insulating behavior, i.e., limited movement of charges, is expected. Thus, considering the different transport mechanisms taking place in dielectric materials, we have assessed the electrical conduction of our devices. We found that the best agreement to the experimental data was obtained

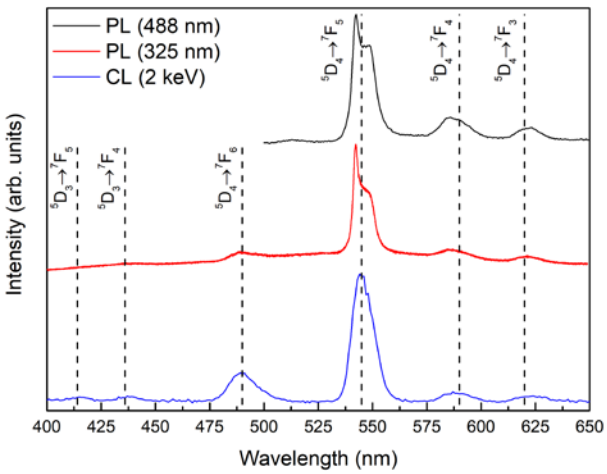

Figure 3 Normalized PL and CL measurements of the $Al/Tb/Al/SiO_2$ structure.

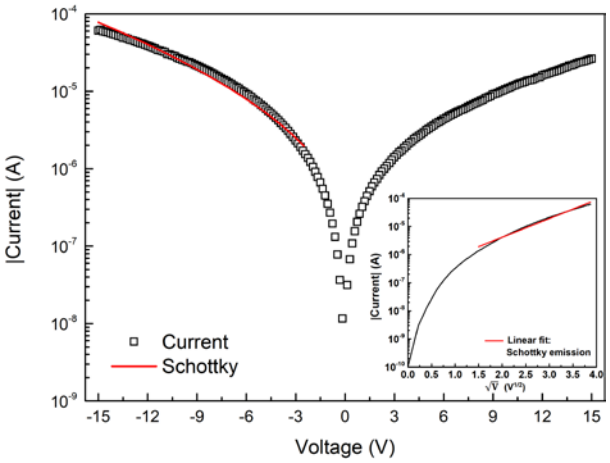

Figure 4 *I*(*V*) curve of the device, fitted taking into account a Schottky type conduction mechanism. The inset shows linearization for Schottky model in the range from -2.25 V to -15 V.

when considering an electrode-limited conduction mechanism based on Schottky emission. Thermionic emission of electrons is achieved when a potential barrier formed at a metal-insulator (or semiconductor-insulator) interface is overcome. Applying an external electric field the barrier can be lowered, easing the emission. This process can be modelled as:

$$J_{\text{Schottky}} = \frac{4\pi m^* q}{h^3} k_B^2 T^2 \exp\left(-\frac{\varphi_b}{k_B T}\right) \exp\left(\frac{\beta}{k_B T} E^{1/2}\right), \quad (1)$$

where φ_B is the potential barrier height in (eV), q the elementary charge, E the applied electric field, $k_B T$ the thermal energy, h the Plank's constant, m^* the effective mass of electrons, and β is defined as:

$$\beta = \sqrt{\frac{q^3}{4\pi\varepsilon_0\varepsilon_r}}, \quad (2)$$

where ε_0 and ε_r are the absolute and relative permittivity, respectively [22].

In the inset of Fig. 4, it is shown the fitting to the experimental *I*(*V*) curve to the Schottky emission model, which yields a relative dielectric constant of the dielectric layer of ε_r = 18.86. However, in general the obtained permittivity value may differ from the experimentally determined values by means of other optical techniques, due to the heterogeneity of our samples. Actually, Poole-Frenkel mechanism is also in good agreement to the experimental data, however with a large dielectric constant (ε_r > 300). The presence of Al in the structure is the probable cause for the Schottky emission fitting best the data, because electrons must overcome the potential barrier generated by the AlO_x layers, as it has been previously reported [23].

The application of an electrical current to the device can also produce the excitation of Tb^{3+} ions, which can be de-excited by emitting their excess of energy in the form of light. The total integrated emission collected by the PMT is shown in Fig. 5(a) and Fig. 5(b) as a function of the applied voltage and current circulating through the device, respectively. We observed that the threshold voltage to observe emission is at 8.5 V, whereas higher voltages produce an almost exponential increase of the integrated EL.

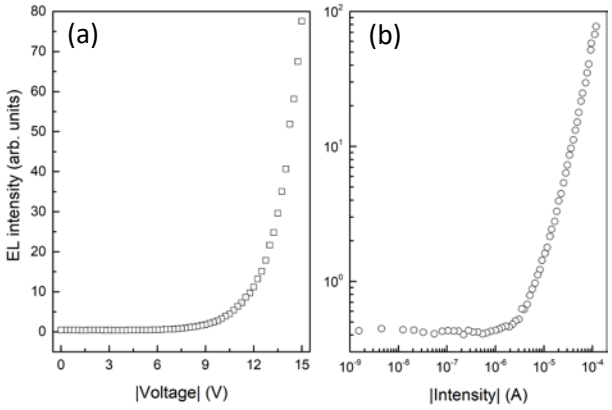

Figure 5 Integrated emission of the Al/Tb/Al/SiO_2 structure, obtained in accumulation, as a function of (a) voltage and (b) current, represented in absolute value.

Looking at the behavior of the EL with the injected current, we observe a threshold current for emission at ≈2 µA, and it increases linearly with the current, which establishes a direct relation between impinging electrons and resulting emitted photons.

The spectral analysis of the EL is displayed in Fig. 6. The spectra were acquired for 30 seconds after applying cycles of -100 µA at -18 V, in the range of 400 – 1100 nm. The spectra exhibit peaks at 437, 483, 531 and 576 nm, over a broad low-intensity background. Whereas the former features correspond to $^5D_4 \rightarrow {}^7F_J$ transitions (with J = 6, 5, 4 and 3) from Tb^{3+} ions, in good agreement to PL and CL measurements (see Fig. 3), the latter band is probably originated in the deep defects in either the SiO_2 or the ITO contact.

Another interesting observation is the fact that there is an intensity reduction of the Tb emission at successive cycles, reaching total quenching of Tb emission beyond five cycles (please see spectrum labeled as cycle 6 in Fig. 6, where only the background contribution is observed). This quenching could be related to some atomic structural rearrangement after high electron flux is injected. Indeed, it

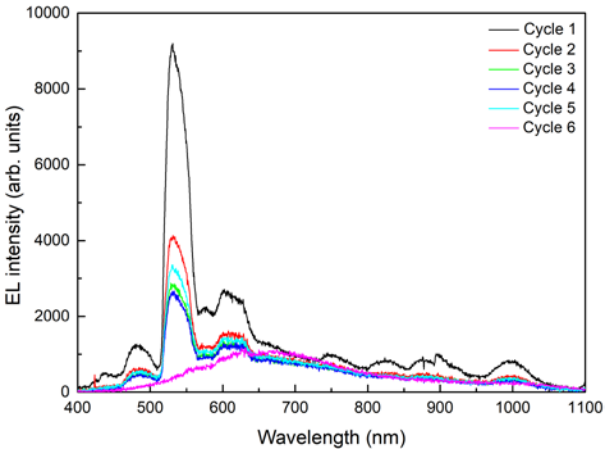

Figure 6 EL spectrum of the device for different cycles of 100 µA and 30 s.

has been observed in oxide matrices that, under certain excitation conditions, a displacement of oxygen atoms takes place [24], [25]. This, in turn, induces both the creation of alternative (oxygen vacancies-related) conduction paths and the probable reduction of Tb-O bonds, the latter reducing the concentration of optically-active centers. In this frame, an increase of the thermal budget could improve the stability of the Tb_2O_3 phase, making this material a potential candidate for future optoelectronics applications, in particular as integrated light emitting devices.

4 Conclusions

Al/Tb/Al/SiO_2 nanomultilayers have been fabricated by electron beam evaporation, alternatively depositing each layer. Optical characterization by means of PL and CL showed that Tb^{3+} ions are optically active. Electrical characterization allowed inferring that the conduction mechanism governing the structure is a Schottky emission model, although thermal activated mechanisms cannot be discarded. The threshold voltage and current for EL to take place were determine by integrated EL measurement. As well, the spectral distribution of EL is related to a combination between Tb^{3+} ions and matrix defect-related emission. The hereby presented results prove that the combination of electron beam evaporation and nanomultilayer structures are useful to obtain luminescent Al/Tb/Al/SiO_2 light-emitting systems.

Acknowledgements This work was financially supported by the Spanish Ministry of Economy and Competitiveness (TEC2016-76849-C2-1-R). O.B. also acknowledges the subprogram "*Ayudas para Contratos Predoctorales para la Formación de Doctores*" from the Spanish Ministry of Economy and Competitiveness for economical support

References

[1] "Efficient blue light-emitting diodes leading to bright and energy-saving white light sources", The Nobel Prize in Physics 2014 - Advanced Information, [online], *Nobel Media AB*, Available: http://www.nobelprize.org/nobel_prizes/physics/laureates/2014/advanced.html, 2014; Accessed: 10/06/2017.
[2] K. D. Hirschman, L. Tsybeskov, S. P. Duttagupta and P. Fauchet, *Nature*, vol. 384, no. 6607, p. 338, November 1996.
[3] G. T. Reed, G. Mashanovich, F. Y. Gardes and D. J. Thomson, *Nature photonics*, vol. 4, no. 8, pp. 518-526, July 2010.
[4] D. J. Miller, P. M. Watts and A. W. Moore, *Proceedings of the 5th ACM/IEEE Symposium on Architectures for Networking and Communications Systems*, ACM, pp. 94-103, 2009.
[5] S. Yerci, R. Li, and L. Dal Negro, *Applied Physics Letters*, vol. 97, no. 8, p. 081109, August 2010.
[6] A. J. Kenyon, *Progress in Quantum Electronics*, vol. 26, no. 4, pp. 225-284, October 2002.
[7] Shibin Jiang (Ed.), *Proceedings of the SPIE VII Conference on Rare-Earth Doped Materials and Devices*, vol. 4990, June 2003.
[8] J. Li, O. H. Zalloum, T. Roschuk, C. L. Heng, J. Wojcik and P. Mascher, *Advances in Optical Technologies*, March 2008.
[9] A. J. Kenyon, P. F. Trwoga, M. Federighi and C. W. Pitt, *Journal of Physics: Condensed Matter*, vol. 6, no. 21, L319-L324, March 1994.
[10] J. M. Ramírez, Y. Berencén, L. López-Conesa, J. M. Rebled, F. Peiró and B. Garrido, *Applied Physics Letters*, vol. 103, no. 8, p. 081102, August 2013.
[11] Y. Berencén et al., *Applied Physics Letters*, vol. 103, no. 11, p. 111102, September 2013.
[12] S. Boninelli, G. Bellocchi, G. Franzò, M. Miritello and F. Iacona, *Journal of Applied Physics*, vol. 113, no. 14, p. 143503, April 2013.
[13] A. J. Silversmith, D. M. Boye, K. S. Brewer, C. E. Gillespie, Y. Lu, and D. L. Campbell, *Journal of luminescence*, vol. 121, no. 1, pp. 14-20, November 2006.
[14] P. Ruterana, M. P. Chauvat and K. Lorenz, *Semiconductor Science and Technology*, vol. 30, no. 4, p. 044004, March 2015.
[15] J. L. Deschanvres, W. Meffre, J. C. Joubert, J. P. Senateur, F. Robaut, J. E. Broquin and R. Rimet, *Journal of alloys and compounds*, vol. 275, pp. 742-745, September 1998.
[16] T. Minami, T. Yamamoto and T. Miyata, *Thin Solid Films*, vol. 366, no. 1, pp. 63-68, January 2000.
[17] X. P. Zhao and J. B. Yin, *Chemistry of Materials*, vol. 14, no. 5, pp. 2258-2263, February 2002.
[18] L. Norin, E. Vanin, P. Soininen and M. Putkonen, in *Conference on Lasers and Electro-Optics*, Optical Society of America, May 2007.
[19] O. Blázquez, J. M. Ramírez, J. López-Vidrier, Y. Berencén, S. Hernández, P. Sanchis and B. Garrido, in *SPIE Microtechnologies*, pp. 95200K-95200K, International Society for Optics and Photonics, June 2015.
[20] O. Blázquez et al., *Journal of Applied Physics*, vol. 120, no. 13, p. 135302, October 2016.
[21] H. S. Ahmed, O. M. Ntwaeaborwa, M. A. Gusowski, J. R. Botha, and R. E. Kroon, *Physica B: Condensed Matter*, vol. 407, no. 10, pp. 1653-1655, May 2012.
[22] J. M. Ramírez, Ph.D. thesis, Dept. d'Electrònica, University de Barcelona, Barcelona, Spain, June 2015.
[23] C. J. Li, S. Jou, and W. L. Chen, *Japanese Journal of Applied Physics*, vol. 50, no. 1S2, p. 01BG08, January 2011.
[24] I. Valov, *ChemElectroChem*, vol. 1, no. 1, pp. 26-36, January 2014.
[25] E. W. Lim, and R. Ismail, *Electronics*, vol. 4, no. 3, pp. 586-613, September 2015.